Cellulose (2021) 28:3097–3112
https://doi.org/10.1007/s10570-021-03720-1

ORIGINAL RESEARCH

Enhanced electrolyte retention capability of separator for lithium-ion battery constructed by decorating ZIF-67 on bacterial cellulose nanofiber

Qiumei Huang · Chuanshan Zhao · Xia Li

Received: 27 August 2020 / Accepted: 22 January 2021 / Published online: 3 February 2021

Abstract The separator is a key component of the lithium-ion battery (LIB), which not only prevents the anode and the cathode from contacting, but is also related to the performance of the LIB. However, the widely used polyolefin separator has the disadvantages of inferior electrolyte retention capability and poor electrolyte wettability. Therefore, the development of high-performance separators for LIB has attracted widespread attention. In order to enhance the electrolyte retention capacity of the separator, the bacterial cellulose (BC)/zeolitic imidazolate framework-67 (ZIF-67) composite separator was prepared by introducing ZIF-67 on the BC nanofibers. It was found that the introduction of ZIF-67 in BC membrane significantly improved the pore structure and enhanced the electrolyte retention capability, thus contributing to the transfer of lithium-ion, increasing the ionic conductivity (0.837 mS cm^{-1}). In terms of ionic conductivity, BC/ZIF-67 separator has achieved a great improvement compared to polypropylene (PP) separator (0.096 mS cm^{-1}). Besides, the prepared BC/ZIF-67 composite separators hardly shrink at high temperatures. The discharge capacity retention of the LIB using BC/ZIF-67 separator was 91.41% after 100 cycles (0.2 C). Meanwhile, LIB with BC/ZIF-67 separator showed a large discharge capacity (156 mAh g^{-1}) and improved rate performance. Therefore, the BC/ZIF-67 composite membrane has good development potential in the direction of LIB separator.

Supplementary Information The online version contains supplementary material available at https://doi.org/10.1007/s10570-021-03720-1.

Q. Huang · C. Zhao (✉) · X. Li
State Key Laboratory of Biobased Material and Green Papermaking, Qilu University of Technology, Shandong Academy of Sciences, Jinan 250353, China
e-mail: ppzcs78@163.com

Q. Huang
e-mail: cthqmch@163.com

X. Li
e-mail: sqlixia126@126.com

Graphic abstract

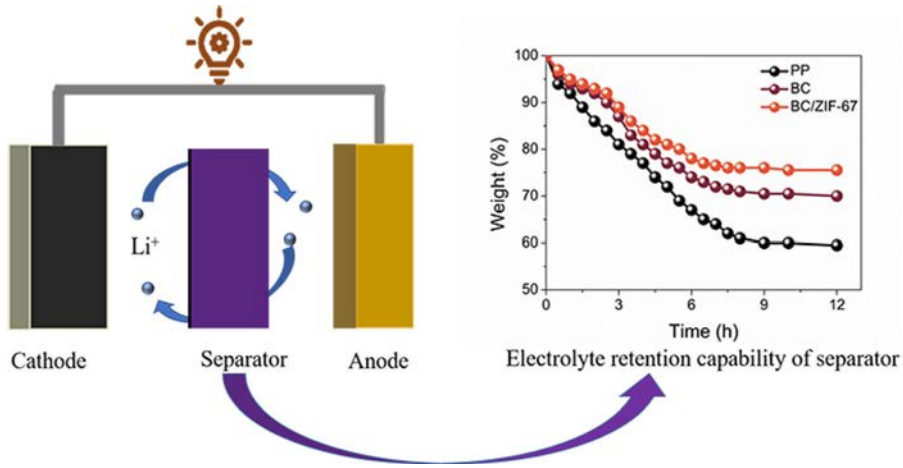

Keywords Lithium-ion battery separator · Bacterial cellulose nanofiber · ZIF-67 · Electrolyte retention capability · Wettability

Introduction

In order to save energy and reduce emissions, the development of renewable energy has attracted worldwide attention. (Wang et al. 2020). Lithium-ion battery (LIB) is a critical element in the development of renewable energy. It has been widely used in electric vehicles, aerospace technology, and portable electronic devices (Reizabal et al. 2020; Sun et al. 2020a). separator is an essential component of LIB. It can not only block the direct contact between the cathode and anode, but also affect the cycle stability and specific capacity of the LIB. In addition, the migration of lithium-ions between the cathode and anode benefits from the fact that the separator can carry electrolyte. In a word, the performance of separator will strongly influence the electrochemical performance of LIB (Costa et al. 2019; Zhu et al. 2020).

For now, microporous polyolefin separator has been widely used because of their easy large-scale production, low cost, and high mechanical strength. However, some disadvantages of polyolefin separators limit the wide application of LIB (He et al. 2020; Zhao et al. 2020). The limitations of polyolefin separators include environmentally unfriendly, poor surface wettability, and low thermal stability. Therefore, research on separators with environmentally friendly, good electrolyte affinity, and high temperature resistance characteristics has become an important part of the development of LIB (Chen et al. 2020; Xue et al. 2020). In order to improve the performance of polyolefin separator, some researchers have adopted the method of coating or atomic layer deposition on the surface (Jeong et al. 2010b; Moon et al. 2019; Zhang et al. 2019b). Disappointingly, the inorganic particles in the coating were easily peeled off from the separator during the LIB assembly or operation process (Fang et al. 2011), and the adhesive may block the pores of the separator during the coating process, which would affect performance of LIB (Shi et al. 2019).

Currently, the adoption of renewable eco-friendly materials to replace the materials that pollute the environment in LIB has raised considerable attention. Cellulose is extremely abundant natural polymer, which has the advantages of renewability, biocompatibility, degradability (Carlmark et al. 2012). For the past few years, cellulose-based materials have been used as battery separators because of high thermal stability, good wettability to electrolyte, and lightweight. For example, Jia et al. used a simple papermaking technique to combine xonotlite nanowires with wood pulp fibers to develop separator with heat

resistance properties (Jia et al. 2020). Wang et al. sprayed aluminum oxide particles on both sides of the paper-based material composed of cellulose to address the problem of safety (Wang et al. 2018). Despite their high thermal stability, the separator was thicker and the pore size was too large. Therefore, their application in LIB is limited.

Cellulose nanofibers (CNFs) have a smaller diameter, which could improve the pore size of the separator (Zhang et al. 2019a). Sheng et al. prepared an ultra-light and ultra-thin cellulose nanofibril separator by vacuum filtration of cellulose nanofibril, which showed thinner thickness, appropriate pore size, and better electrochemical properties (Sheng et al. 2020). Bacterial cellulose (BC) is a macromolecular compound synthesized from some microorganisms, and its chemical composition is similar to that of natural cellulose. Structurally, BC is composed of ribbon-like fibrils with a diameter of about 40 nm and presents a crisscross network structure (Bu et al. 2018). BC has many intriguing properties, such as adequate porosity, excellent electrolyte affinity, and good flexibility. It has been widely concerned in the fields of LIB separator. For instance, Huang et al. reported TEMPO-oxidized BC nanofiber separator with small interfacial resistance (Huang et al. 2020). Jiang et al. directly used dried BC as the separator for LIBs, and the battery exhibited good electrochemical performance (Jiang et al. 2015). However, the hydrogen bond between BC nanofibers reduces the porosity of separator. The lower porosity has a negative impact on the electrolyte uptake and electrolyte retention capacity of the separator. The lack of electrolyte will cause greater interface resistance, thereby reducing the ion conductivity of the separator.

In order to solve the problem of poor electrolyte retention capacity of LIB separator, zeolitic imidazolate framework-67 (ZIF-67) with developed pores and BC with network structure were selected as the raw materials of the separator. In recent years, ZIF-67 has gained substantial attention. It is a novel metal–organic framework coonsist of metal ions (Co^{+}) and organic ligands (2-methylimidazole, Hmim). ZIF-67 is widely used in catalysis, sensing, drug delivery and other fields because of its developed specific surface area and abundant pore structure (Lin et al. 2016; Tran et al. 2011). Sun et al. decorated ZIF-67 on CNFs and successfully prepared ZIF-67@CNF composite separator with improved pore structure (Sun et al. 2020a, b). However, mechanical processing was required in the process of preparing CNFs, which resulted in high energy consumption. In addition, when synthesizing ZIF-67 on nanofibers, CNFs must be uniformly dispersed. If CNF is not uniformly dispersed, it will cause uneven pore size of the separator after molding.

BC has high crystallinity and excellent liquid retention ability, and the fiber diameter is about 50 nm. BC nanofibers feature an abundance of hydroxyl groups, which provide copious reaction sites for nucleation, growth and adhesion of ZIFs crystal (Zhu et al. 2018). Herein, we directly adorned BC nanofibers with ZIF-67 by in-situ growth to prepare BC/ZIF-67 composite separator for LIB. The difference from previous research is that we synthesized ZIF-67 on the BC wet membrane to improve the electrolyte retention capability of the separator, and our research method does not involve the preparation of CNFs, which is relatively simple and has low energy consumption. The introduction of highly porous ZIF-67 on BC nanofibers can not only prevent the aggregation of nanofibers, but also improve the electrolyte retention capability, which will facilitate the transport of lithium-ion. Hence, BC/ZIF-67 composite separator shows lower interface resistance, higher ion conductivity, and preferable cycle performance. The micromorphology, electrolyte wettability, thermal stability, and cycling performance of the separator were studied in detail, which proves that the BC/ZIF-67 composite separator has a good development prospect.

Experiment

Materials

BC wet film was purchased from Yide Food Co., Ltd. Sodium hydroxide (96%), anhydrous ethanol, methanol (99.5%), n-butanol (99%), N-methyl-2-pyrrolidinone (NMP, 99.9%), $Co(NO_3)_2{\cdot}6H_2O$ (99%), and Hmim ($C_4H_6N_2$, 98%) were provided by Aladdin Industrial Corporation. Lithium iron phosphate ($LiFePO_4$), polyvinylidene fluoride (PVDF), conductive carbon (Super P Li), Aluminum foil and lithium (Li) metal anodes were supplied by Shenzhen Lizhiyuan Intelligent Technology Co., Ltd. The conventional liquid electrolyte 1.0 M lithium

hexafluorophosphate ($LiPF_6$) was obtained from Kelude Company. The solvent of this electrolyte is ethylene carbonate/dimethyl carbonate (1:1 by volume). PP separator was purchased from Celgard Company and used for comparative analysis. All the reagents were used without further purification.

Ionic interaction of BC with Co^{2+}

BC hydrogels were purified by boiling in 1 M sodium hydroxide solution for 1 h at 60 °C, and then washed several times until it was neutral. The treated BC hydrogels were immersed in anhydrous ethanol for 24 h. In a typical experiment, BC gels (2 cm × 2 cm) were soaked in $Co(NO_3)_2{\cdot}6H_2O$/methanol solution (0.052 M) and stirred at 500 rpm for 24 h at room temperature. The obtained metal-chelated gels were called BC-Co^{2+} gels.

Preparation of BC/ZIF-67 composite separators

BC-Co^{2+} gels were washed three times with methanol. The gels were then immersed in Hmim/methanol solution (0.414 M) under vigorous stirring for 20 min and aged for 24 h at room temperature for the growth of ZIF-67. The synthesized composite material was rinsed by anhydrous ethanol for several times and vacuum dried at 95 °C for 30 min to obtain BC/ZIF-67 composite separators. For comparison, ZIF-67 particles were synthesized by mingling of $Co(NO_3)_2{\cdot}6H_2O$/methanol solution (0.052 M) and 0.414 M Hmim/methanol solution at 25 °C for 24 h. The pure BC membrane was treated according to the above steps.

Preparation of coin cell

Firstly, the cathode of the cell was made of $LiFePO_4$, conductive carbon, and PVDF with a mass ratio of 8:1:1 in NMP. The obtained $LiFePO_4$ uniform slurry was cast on an aluminum foil (20 μm thickness) and dried at 80 °C for 12 h in a vacuum oven. Then, the dried $LiFePO_4$ cathode was cut into a 16 mm diameter disk and weighed. Secondly, in order to test the battery performance, 2032-type coin cells were assembled, which mainly includes $LiFePO_4$ cathode, lithium metal anode, $LiPF_6$ electrolyte, and separators. Finally, the cells were sealed by a hydraulic sealing machine (DISIPU Corporation, disperse, China) under 1000 psi assembling pressure.

Material characterization

Scanning electron microscope (SEM, Regulus-8220, Hitachi, Japan) was used to obtain the morphology of the sample. The XRD spectra of the separators were measured by X-ray diffractometer (D8-ADVANCE, Bruker, Germany). The FTIR spectra of separators

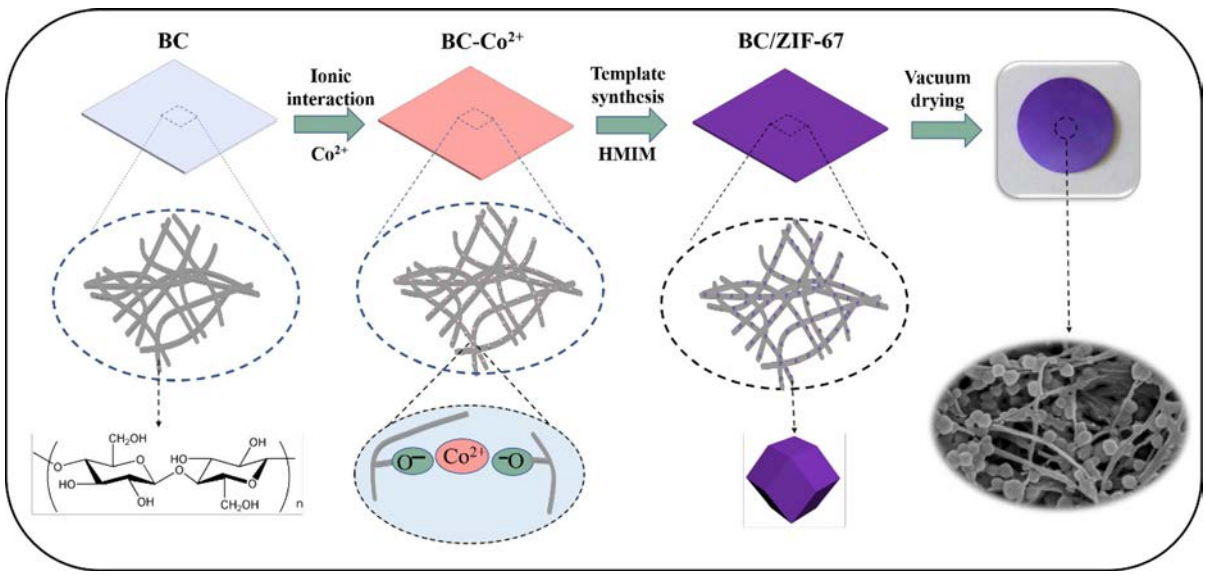

Fig. 1 Schematic of the synthesis of BC/ZIF-67 composite separators

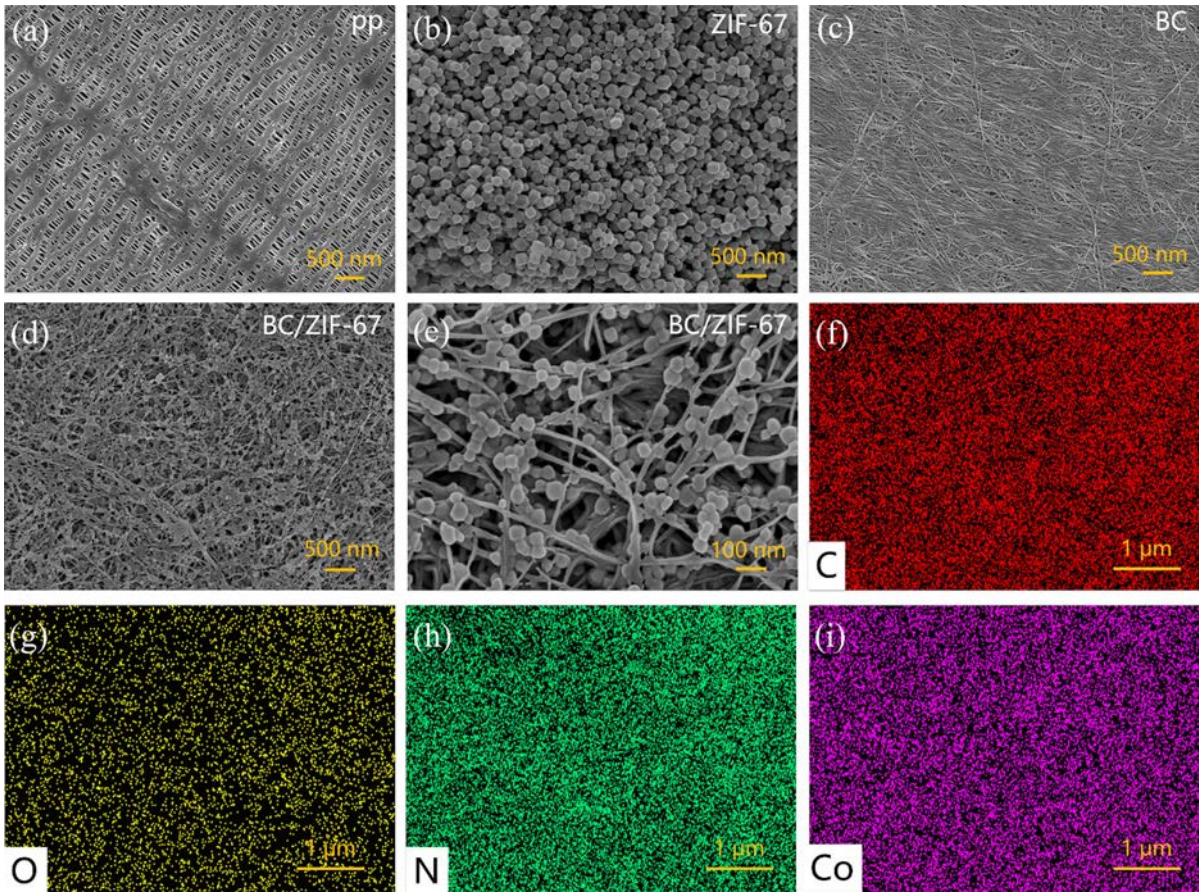

Fig. 2 **a** SEM images of the PP separators; **b** SEM images of the ZIF-67 particles; **c** SEM images of the BC separators; **d** and **e** SEM images of the BC/ZIF-67 separators; **f**, **g**, **h**, and **i** EDX elemental mapping images of the BC/ZIF-67 separators

were measured by the ALPHA infrared spectrometer with a range of 4000–500 cm^{-1}. The thermal stability of separator was analyzed by synchronous thermal analyzer (STA449F3, NETZSCH, Germany). The specific weight loss rate of samples was determined by derivative thermogravimetric (DTG) curve. Contact angle measuring instrument (OCA50, Dataphysics, Germany) was used to measure the wettability of the sample. The organic electrolyte uptake and desorption rate of the sample were measured at room temperature. The absolutely dried separator (mass W_0) was soaked in 1.0 M $LiPF_6$ liquid electrolyte for a certain period of time, then the excess electrolyte was removed and the weight of the wet separator (W_1) was measured. After the separator was immersed in an organic electrolyte for 2 h, the obtained separator (W_2) was placed at 25 °C and 50% relative humidity, and the weight (W_3) of each separator was monitored over time. The electrolyte uptake (W_t) and desorption (W_t') rate of the separator were determined by the followed equations:

$$W_t = \frac{W_1 - W_0}{W_0} \times 100\% \quad (1)$$

$$W_t' = \frac{W_3}{W_2} \times 100\% \quad (2)$$

The separator was immersed in the n-butanol solution and its porosity was calculated by the following formula as follows:

$$\text{Porosity} = \frac{W_m - W_b}{\rho_b V_p} \times 100\% \quad (3)$$

where W_m and W_b are the weight of separator before and after immersed in n-butanol solution for 1 h, ρ_b and V_p are respectively the density of n-butanol

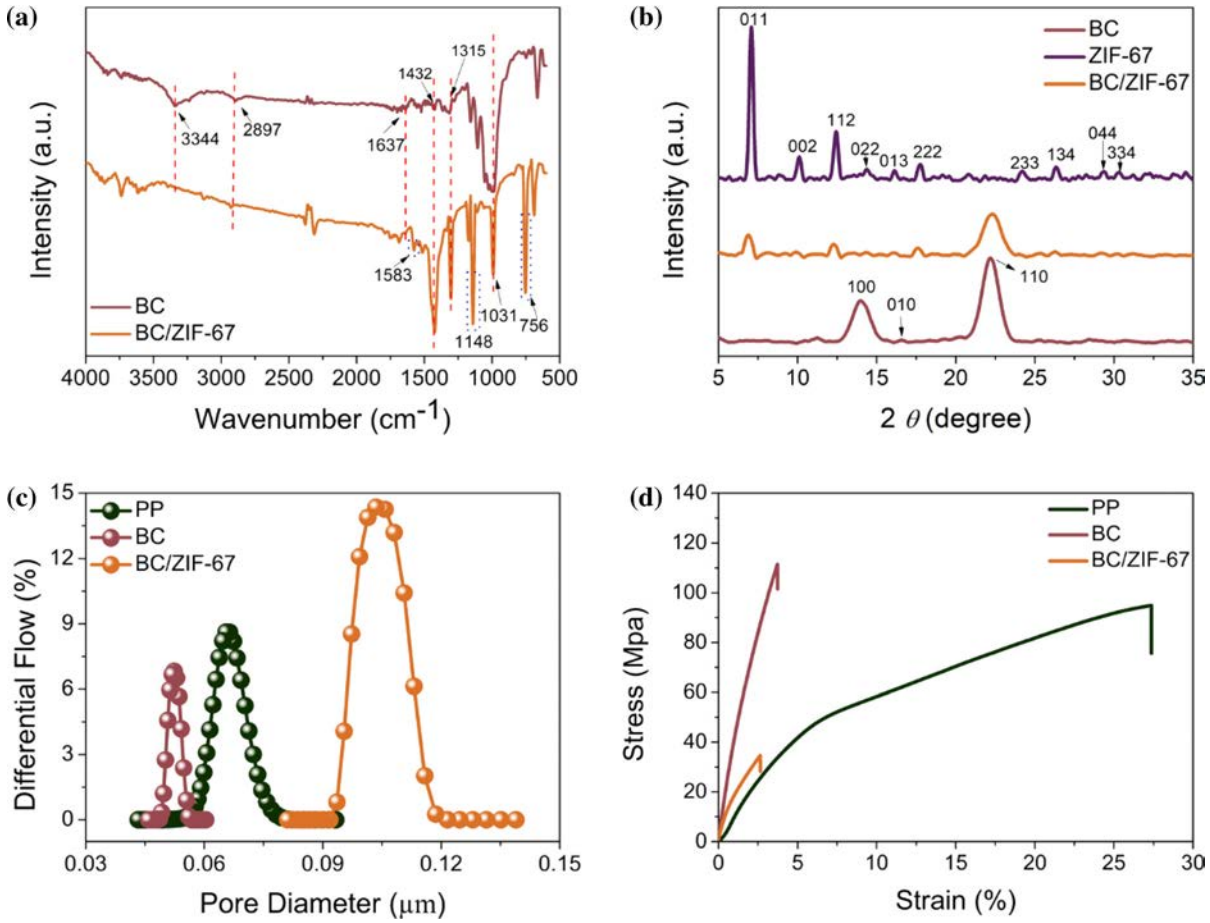

Fig. 3 **a** FTIR spectra of BC and BC/ZIF-67 separators; **b** XRD patterns of the separators; **c** pore size distribution of the separators; **d** mechanical property of the separators

solution and the volume of dry separator. The mechanical property of the separators were tested at room temperature on a texture analyzer (Ta.XT Plus, SMS, UK) with separator in the size of 1.5 cm × 4 cm. A membrane pore size analyzer (Porometer 3G, Quantachrome, USA) was used to analysis the pore size of the separators.

Electrochemical measurements

An electrochemical workstation (P4000A, PARSTAT, USA) was used to conduct cyclic voltammetry curves (CV), electrochemical impedance spectroscopy (EIS), chronoamperometry (CA) profile, and linear sweep voltammetry (LSV) measurement. Before making any measurement, the cell was aged for 24 h to ensure that the electrolyte completely penetrated into the electrodes.

The stainless steel (SS) plate was used as the working electrode and symmetrical electrode of the battery, and the bulk resistance of the separators were tested in the range of 0.1–10^5 Hz. Using the same method, lithium metal electrode was used as the working electrode and symmetrical electrode to test the interfacial resistance of separator. The ionic conductivity was calculated based on the following equation:

$$\sigma = \frac{L}{A} \times R \tag{4}$$

where σ (mS cm^{-1}) is the ionic conductivity, R (Ω) is the bulk resistance determined, L (cm) is the thickness of separators, A (cm^{-2}) is the area of SS electrodes. SS was used as the working electrode and lithium metal was used as the reference electrode to measure the linear sweep voltammetry (LSV) curves

in the voltage range of 3.0 to 5.5 V. Lithium-ion transference number (t +) was calculated by testing the CA curve of Li/separator/Li half-cell and the EIS before and after polarization (Xu et al. 2018). The cycle performance and rate performance of coin cell were tested by LAND test system (CT2001A, Wuhan, China).

Results and discussion

Morphology and structure

The synthesis process of the BC/ZIF-67 composite separators are schematically illustrated in Fig. 1. The composite separators scaffolded by BC nanofibers were successfully prepared by ionic interaction, template synthesis of ZIF-67, and vacuum drying. When the purified BC hydrogels were exposed to $Co(NO_3)_2{\cdot}6H_2O$ solution, the O–H group of BC nanofibers was beneficial to the adsorption of Co^{2+}, thus forming BC gels rich in Co^{2+} (BC-Co^{2+}). When the BC-Co^{2+} gel was placed in the organic ligand (Hmim) solution, ZIF-67 was synthesized on the BC nanofiber. The presence of O–H groups on BC nanofibers provided binding sites for ZIF-67 (Guo et al. 2020).

The SEM image of all samples are illustrated in Fig. 2a–e. As PP separator was stretched in the machine direction (MD) at high temperature, flat pore structure was observed in Fig. 2a. In the process of stretching PP separator, there may be local tearing of slit pores. Figure 2b shows that the particle size of ZIF-67 is about 300 nm. The SEM images of ZIF-67 particles indicated their rhombic dodecahedron morphology. The ZIF-67 particles have good affinity for electrolyte and distinctly porous structures, so the BC/ZIF-67 composite separators to store more electrolytes (Chen et al. 2018). The network structure of the BC separators was composed of continuous and entangled nanofibers (Huang et al. 2020). The relatively dense structure of BC separators is observed in Fig. 2c, which could slow down the lithium-ion migration rate and affect the electrochemical performance of the LIB (Weng et al. 2015). As shown in Fig. 2d, the pores with relatively uniform distribution can be observed in the BC/ZIF-67 composite separators. Figure 2e shows the successful synthesis of ZIF-67 particles on BC nanofibers. Owing to the high aspect ratio of BC nanofibers, the nucleation of ZIF-67 would compete with the growth of ZIF-67, so the ZIF-67 (80–100 nm) were smaller than that ($\sim$ 300 nm) synthesized without the presence of BC-Co^{2+}. In addition, ZIF-67 were decorated on BC nanofibers, which prevented the formation of hydrogen bonds between fibers to some extent (Hishikawa et al. 2017). It changed the original compact structure and formed suitable pores, which may increase the lithium-ion transport rate. The EDX spectra of BC/ZIF-67 composite separators were provided in Fig. 2f–i. The atomic percentages of carbon, nitrogen, oxygen, and cobalt were 60.16, 28.67, 3.79, and 7.37, respectively. Both BC and ZIF-67 particles contain carbon atoms (Fig. 2f). Figure 2h, i show that N and Co element were uniformly distributed in the BC/ZIF-67 composite separator, which indicated that ZIF-67 has successfully grown on BC nanofibers. The atomic ratio of nitrogen/cobalt was 28.67/7.37, which is about 3.89 and similar to the atom ratio ZIF-67 ($C_8H_{10}N_4Co$).

The FTIR spectra of BC and BC/ZIF-67 separators were measured to evaluate the chemical structure between BC and BC/ZIF-67 (Fig. 3a). Due to the formation of ZIF-67 on BC nanofibers, there are mainly three distinct different peaks (highlighted by blue rectangles) between the BC and BC/ZIF-67 separators. The characteristic peaks of ZIF-67 were mostly derived from Hmim. The peak at 1583 cm^{-1} was related to the C=N stretching vibration of Hmim (Qin et al. 2017). The peaks at 1148 cm^{-1} and 756 cm^{-1} were related to the stretching vibration and bending vibration of the imidazole ring, respectively (Hu et al. 2011). Due to the typical cellulose I structure of BC, some peaks of BC/ZIF-67 and BC separators were similar. The peaks at 3000–3660 cm^{-1} were associated with O–H stretching vibration. The peak at 3344 cm^{-1} was related to the inter-molecular H bonds (Tian et al. 2014). The peak at 2897 cm^{-1} was considered as C–H stretching vibration of the BC. The peaks at 1637, 1432, 1315, and 1031 cm^{-1} were associated with C=O stretching vibration, CH_2 symmetric vibration, CH_2 wagging vibration, C–O stretching vibration. Figure 3b shows the XRD curves of the samples. The characteristic peaks (2θ) of the BC located at about 14.2°, 16.5°, and 22.6°, which corresponded to (100), (010), and (110) planes, respectively (French 2014). In the ZIF-67 particles, strong diffractions at 2θ of 7.09°, 10.11°, 12.52°, and 17.82° assigned to (011), (002), (112), and

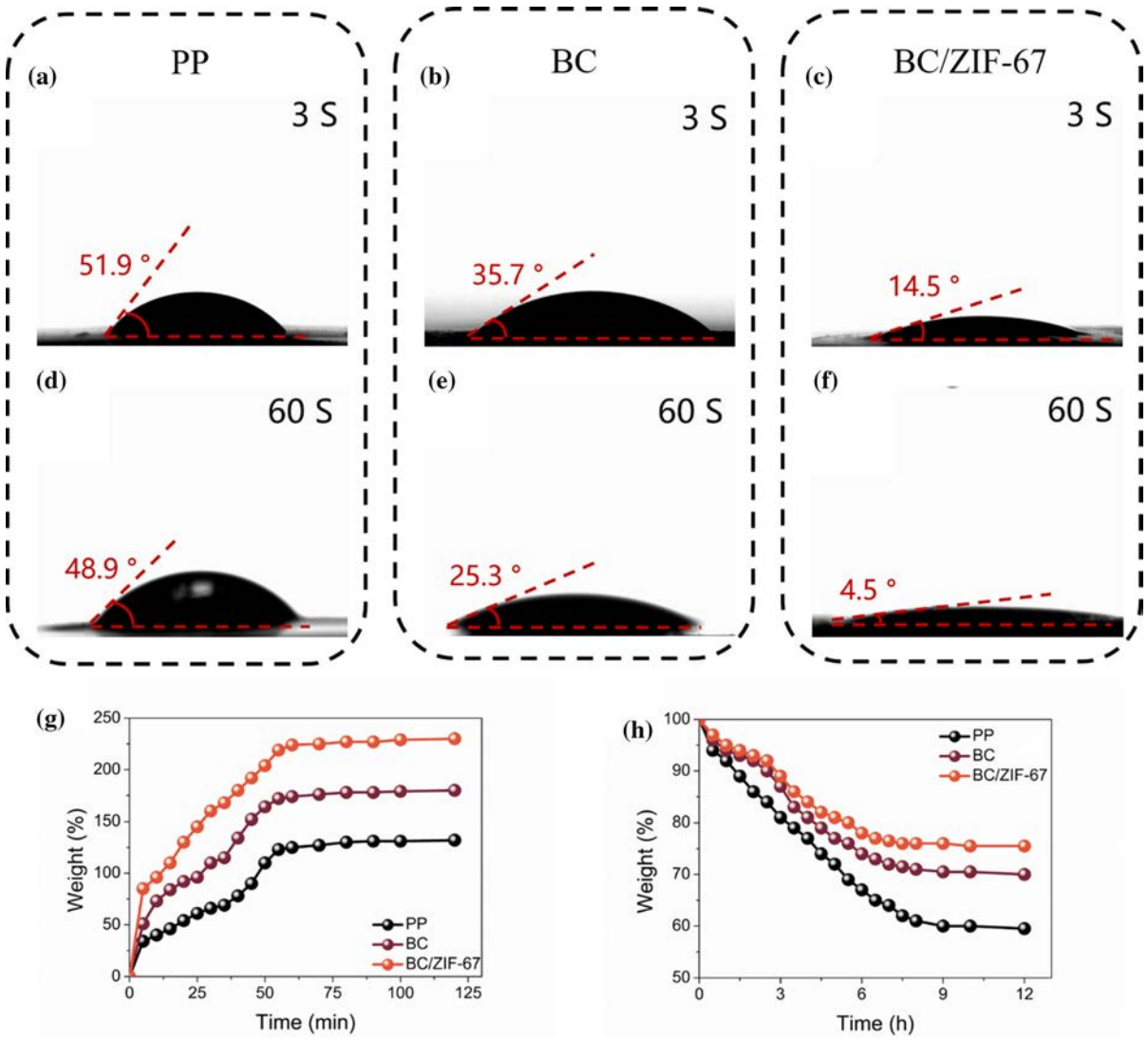

Fig. 4 Contact angle images of the separators after dripping electrolyte for 3 s **a–c** and 30 s **d–f**; **g** electrolyte desorption of and **h** electrolyte retention of the PP, BC, and BC/ZIF-67 separators as functions of time

Table 1 The relevant parameters of PP, BC, and BC/ZIF-67 separators

Sample	Thickness (μm)	Porosity (%)	Wettability	Electrolyte uptake (%)	Ionic conductivity (mS cm^{-1})	t^+
PP	25	41	Poor	132	0.096	0.316
BC	20	59	Good	180	0.128	0.463
BC/ZIF-67	72	68	Better	230	0.837	0.543

(222) diffraction peaks were higher than the other peaks (Sun et al. 2020a, b). The BC, ZIF-67, and BC/ZIF-67 showed similar XRD patterns, indicating that ZIF-67 crystals were formed in the BC membranes. However, the diffraction peak intensity of BC/ZIF-67 separators became weak. The main reason was that the existence of fibers hindered the growth of ZIF-67,

which reduced the crystallinity of the BC/ZIF-67 composite separators.

A membrane pore size analyzer was used to measure the pore size of the separators. It starts by filling the pores with a special wetting fluid. Gas pressure empties pores according to size, and the resulting flow through the pores is measured. The average pore diameters of PP, BC, and BC/ZIF-67 separators were 66, 53, and 104 nm (Fig. 3c). The average pore diameter of BC membrane grew larger after being decorated with ZIF-67. The average pore size of the BC/ZIF-67 separator was much smaller than the results in the previously published articles (Reizabal et al. 2020). The mechanical properties of PP, BC, and BC/ZIF-67 separators were showed in Fig. 3d. The tensile stresses for PP, BC, and BC/ZIF-

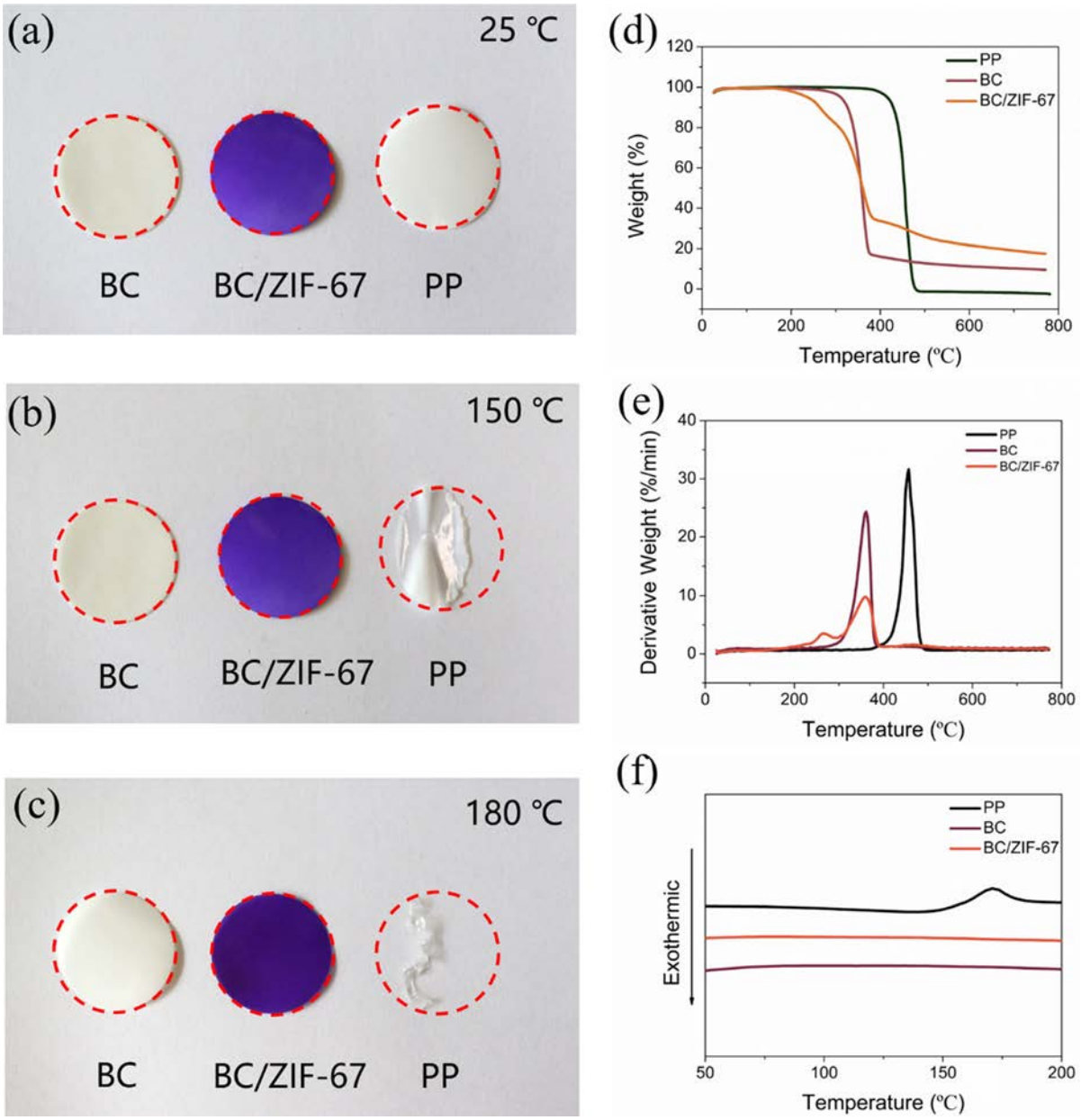

Fig. 5 Photographs of the BC, BC/ZIF-67, and PP separators **a** befor and after heat treatment at **b** 150 °C and **c** 180 °C for 1 h, respectively; **d** TGA, **e** DTG, and **f** DSC curves of the BC, BC/ZIF-67, and PP separators

67 separators were 94.8, 110.6, and 34.2 MPa, respectively. The mechanical properties of BC separators were mainly derived from the hydrogen bonds formed between fibers during drying (Zhou et al. 2013). The reduction of tensile strength of BC/ZIF-67 composite separators were mainly affected by two factors. On one hand, the formation of ZIF-67 affected the formation of hydrogen bonds between fibers. On the other hand, the ZIF-67 synthesized on the BC nanofiber prevented the aggregation of the BC nanofiber.

Electrolyte wettability

The affinity of the separator to the organic electrolyte an important parameter because it directly affects the electrochemical performance of LIB (Esho et al. 2018). The outstanding electrolyte wettability could allow quick absorption and retain electrolyte, thereby improving the lithium-ion transmission efficiency. However, the inherent low surface energy performance of PP separator deemed it difficult to absorb electrolyte. Insufficient electrolyte absorbed by the separator would cause the lithium-ion to migrate too slowly during the charging and discharging process, resulting in poor electrochemical performance of the LIB. Liquid electrolyte 1.0 M LiPF6 was used in electrolyte wettability testing. The solvent of this electrolyte is ethylene carbonate/dimethyl carbonate (1:1 by volume). As shown Fig. 4a–f, when the electrolyte was just dropped, the contact angles of PP, BC, and BC/ZIF-67 separators were 51.9°, 35.7°, and 14.5°, respectively. After the electrolyte was dropped for 60 s, the contact angles of PP, BC, and BC/ZIF-67 separator decreased to 48.9°, 25.3°, and 4.5°, respectively. The smaller contact angle indicated better wettability, so the electrolyte affinity of BC/ZIF-67 separator was the best among all samples.

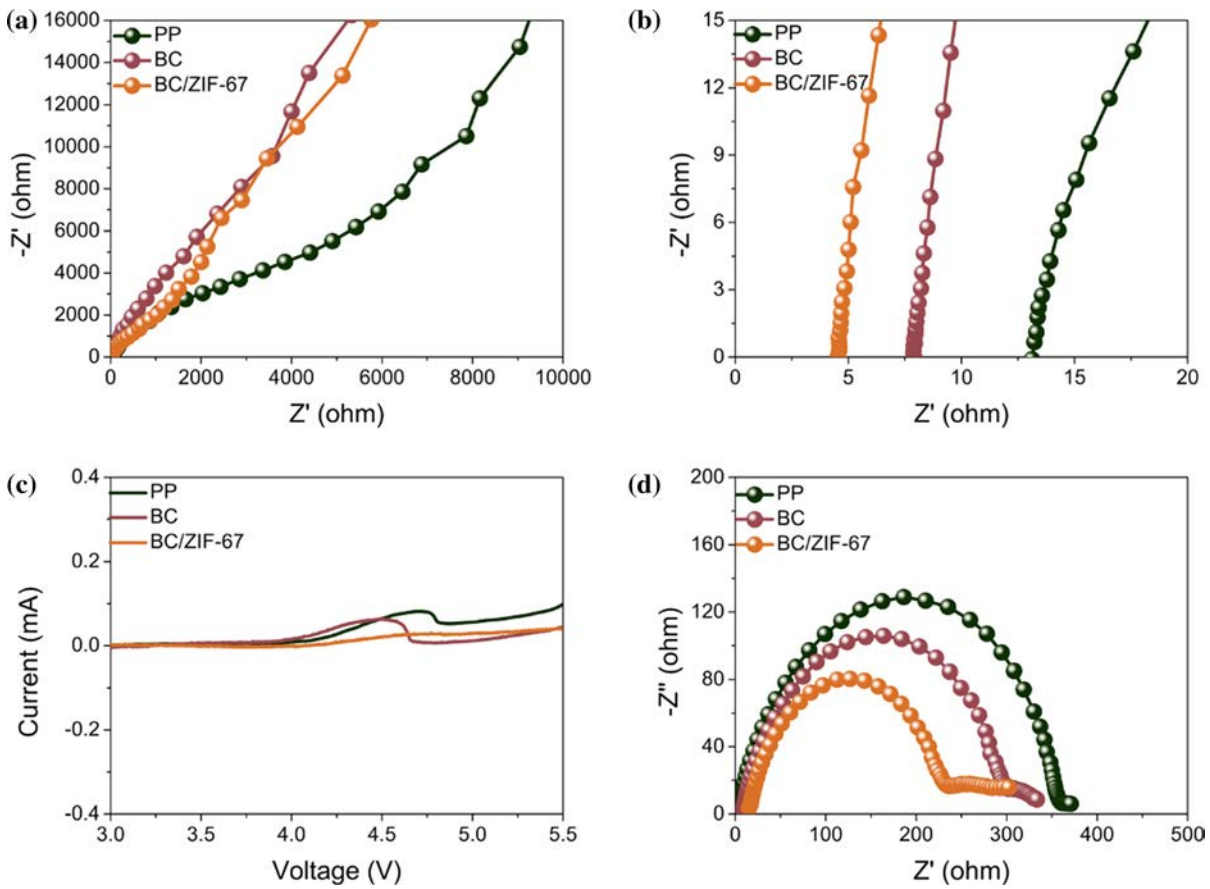

Fig. 6 **a** and **b** AC impedance spectra of SS/separator/SS cells; **c** LSV of SS/separator/Li cells; **d** AC impedance spectra of Li/separator/Li cells

Table 1 summarized the relevant parameters of separators. The electrolyte uptake of PP, BC, and BC/ZIF-67 separators were 132%, 180%, and 230%, respectively. The enhancement of the electrolyte absorption of BC/ZIF-67 separator was mainly benefited from superior porosity and stronger affinity with electrolyte, which could increase the content of organic electrolyte in separator (Li et al. 2014).

Figure 4g shows the changes in electrolyte absorption capacity of PP, BC, and BC/ZIF-67 separators over time. The separators continuously absorbed the electrolyte after being immersed in the electrolyte, and reached saturation in about 120 min. It was observed that BC/ZIF-67 separator had higher electrolyte absorption capacity. The superior electrolyte absorption ability of ZIF-67 separator may be the result of hydrophilicity and surface capillary force. In addition, electrolyte retention capability was also an important property of LIB separator. As shown in Fig. 4h, with the extension of exposure time, the weight of the separator filled with electrolyte lost continuously. The BC/ZIF-67 separator showed the slowest electrolyte loss in exposed air, compared with the PP and BC separators. This was primarily because the ZIF-67 particles had a well-developed pore structure, which allowed the separator to retain more electrolyte (Chen et al. 2018).

Thermal stability

Thermal stability is a significant parameter of the separator, which is related to the safety of LIB. Thermal dimensional stability of separator was studied by thermal shrinkage experiment, as shown in Fig. 5a–c. Evidently, PP separator gradually shrinks with the increase of temperature. The thermal shrinkage ratio of PP separator was approximately 45% at 150 °C and close to 100% at 180 °C. In sharp contrast, the size of BC and BC/ZIF-67 separators did not change significantly even when the temperature rose to 180 °C.

The TGA and DTG curves of PP, BC, and BC/ZIF-67 separators are shown in Fig. 5d, e, respectively. The weight loss before 100 °C was mostly because of the evaporation of water molecules or residual molecules such as methanol or Hmim (Schejn et al. 2014). The initial degradation temperatures ($T_{initial}$) of PP, BC and BC/ZIF-67 separators were about 378 °C, 271 °C and 192 °C, respectively. The maximum degradation temperatures (T_{max}) of PP, BC and BC/ZIF-67 separators were about 456 °C, 361 °C, and 359 °C, respectively. Compared with BC separator, the $T_{initial}$ and T_{max} of BC/ZIF-67 separator was slightly lower. The reason was that the porosity and surface area of the BC membrane were increased after ZIF-67 was grown. The presence of ZIF-67 reduced BC nanofibers accumulation in comparison to the pure BC separators (Sun et al. 2020b). Although the $T_{initial}$ and T_{max} of PP separators were the highest, PP separators had melted before degradation. The char yield (or residual) at 800 °C of PP, BC, and BC/ZIF-67 separators were 0.43%, 11.90%, and 19.86%, respectively. Compared with BC separator, the increase of residual in BC/ZIF-67 separator was due to the synthesis of ZIF-67. The peak at 456 °C was shown the DTG curve of PP separator, which was related to the decomposition of PP. The peak in the range from 300 to 400 °C was attributed to the degradation of BC separator. There were two peaks in the DTG curve of the BC/ZIF-67 separator. The peak from 243°C to 285°C was related to the interaction between cobalt ions and hydroxyl groups (Sun et al. 2021). The other peak was due to the decomposition of BC. Thermal stability of separator was also explored by DSC (Fig. 5f). The peak observed at 168 °C corresponds to the melting point of the PP separator. No peak was observed in DSC curves of BC and BC/ZIF-67 separators, which indicated that their thermal stability was significantly better than that of PP separators. This has played an extremely critical role in improving the safety performance of LIB.

Electrochemical performance

The ionic conductivity of the separator affects the performance of LIB (Zhan et al. 2019). The AC impedance spectra of Fig. 6a, b were used to analyze the bulk resistance. The real axis intercept indicates the bulk resistance of the separator, and the ion conductivity can be obtained by Eq. (4). The bulk resistances of PP, BC, and BC/ZIF-67 separators were 13.06 Ω, 7.76 Ω, and 4.46 Ω, respectively. Correspondingly, the ionic conductivity of PP, BC, and BC/ZIF-67 separators were 0.096 mS cm^{-1}, 0.128 mS cm^{-1}, and 0.837 mS cm^{-1}, respectively. The high ionic conductivities of BC/ZIF-67 separators were due to its superior electrolyte retention capability and porous structure.

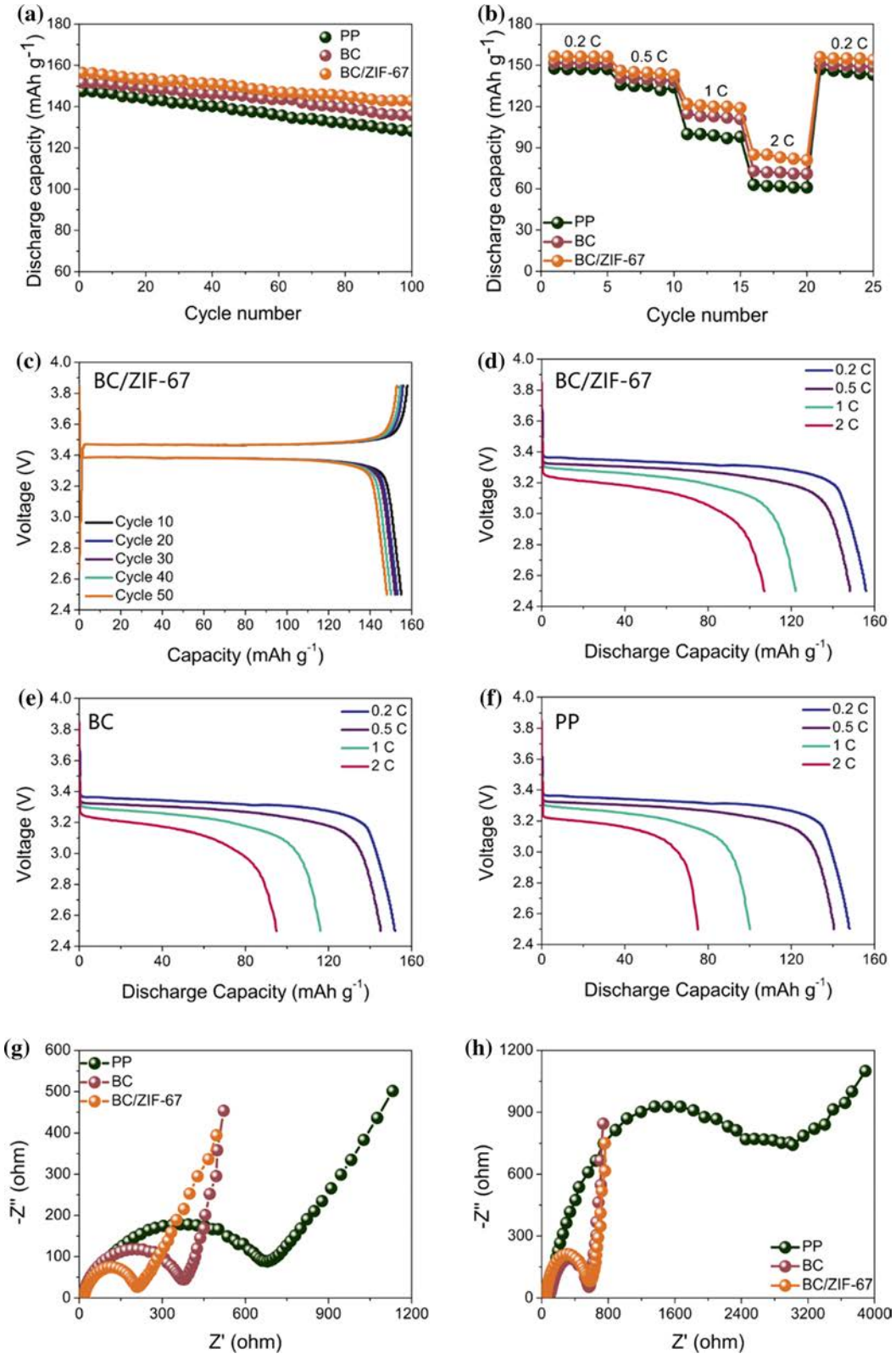
(a)
Discharge capacity (mAh g-1)
Cycle number
PP
BC
BC/ZIF-67
(b)
Discharge capacity (mAh g-1)
Cycle number
0.2 C
0.5 C
1 C
2 C
0.2 C
PP
BC
BC/ZIF-67
(c)
BC/ZIF-67
Voltage (V)
Capacity (mAh g-1)
Cycle 10
Cycle 20
Cycle 30
Cycle 40
Cycle 50
(d)
BC/ZIF-67
Voltage (V)
Discharge Capacity (mAh g-1)
0.2 C
0.5 C
1 C
2 C
(e)
BC
Voltage (V)
Discharge Capacity (mAh g-1)
0.2 C
0.5 C
1 C
2 C
(f)
PP
Voltage (V)
Discharge Capacity (mAh g-1)
0.2 C
0.5 C
1 C
2 C
(g)
-Z'' (ohm)
Z' (ohm)
PP
BC
BC/ZIF-67
(h)
-Z'' (ohm)
Z' (ohm)
PP
BC
BC/ZIF-67

◀**Fig. 7** **a** Cycle performance of the LIB using the PP, BC and BC/ZIF-67 separators at charge/discharge current density of 0.2 C/0.2 C; **b** rate performance of the cells with the PP, BC and BC/ZIF-67 separators at current density of 0.2 C to 2 C; **c** capacity-voltage curves of the cells with BC/ZIF-67 separators at 0.2 C/0.2 C charge/discharge current density; **d** discharge profiles of cells with BC/ZIF-67 separator; **e** discharge profiles of cells with BC separator; **f** discharge profiles of cells with PP separator; Nyquist plots of the cells with PP, BC, and BC/ZIF-67 separator **g** before and **h** after 100 cycles at 0.2 C

The LSV curve of the separator was used to evaluate its electrochemical stability window (Fig. 6c). The corresponding voltage when the current increases sharply was considered as the limit of electrochemical oxidation (Wang et al. 2015). The anodic potential window of PP and BC separators were observed at 4.1 V. No anodic potential window was detected for the BC/ZIF-67 separator until voltage reached 5.5 V, which was indicative of the BC/ZIF-67 separator's better electrochemical stability. This phenomenon was mainly due to the excellent electrolyte retention capacity and wettability of the BC/ZIF-67 separator, which could reduce the decomposition of free solvent molecules and tend to provide a wider electrochemical window for LIB (Chen et al. 2015).

The interfacial resistance of the separator was also measured and shown in Fig. 6d. The semicircle diameter of the AC impedance spectra represented the interface resistance between the separator and the electrode (Xu et al. 2017). The interface resistances of PP, BC, and BC/ZIF-67 separators were 360 Ω, 300 Ω, and 228 Ω respectively. The lower interface resistance of the BC/ZIF-67 separator indicated that the BC/ZIF-67 separator had preferable affinity with the lithium metal electrode. This was related to excellent electrolyte wettability and higher electrolyte retention capacity of BC/ZIF-67 separator, which could promote lithium-ion transport (Huang et al. 2015).

Cell performance

Figure 7a shows the cycling performance of LIBs using PP, BC, and BC/ZIF-67 separators. The first discharge capacity of cells using PP, BC, and BC/ZIF-67 separators were 147 mAh g^{-1}, 151 mAh g^{-1}, and 156 mAh g^{-1}, respectively. After 100 cycles at 0.2 C, the capacity retention of the cells using PP, BC, and BC/ZIF-67 separators were 86.94%, 89.63%, and 91.41%, respectively. The coin cell using BC/ZIF-67 separator had better electrochemical stability and higher capacity retention. This was attributed to the excellent electrolyte retention capability, proper porosity, and fast wetting speed of BC/ZIF-67 separator. After 100 cycles of the LIB, some particles appeared on the PP and BC separator (Fig. S3a-b). These small particles are related to the residual organic carbonate after the electrolyte volatilizes. After the cycle test, no small particles were formed on the surface of the BC/ZIF-67 separator, and ZIF-67 did not fall off the BC nanofibers (Fig. S3c). Therefore, BC/ZIF-67 separator has excellent stability (Sun et al. 2020a, b). The CV curves of the cells are shown in Fig. S1. The oxidation peaks at 3.8 V and reduction peaks at 3.1 V of the cells can be observed, and no other peaks were found. Therefore, the BC and BC/ZIF-67 separator did not affect the operating voltage range. Fig. S2 shows the CA curve and EIS of the sample. The t + of PP, BC, and BC/ZIF-67 separators were 0.316, 0.463, and 0.543, respectively. BC/ZIF-67 separator has the highest t+. This was mainly due to the outstanding electrolyte retention capability and excellent wettability of the BC/ZIF-67 separator.

Figure 7b shows the rate performance of cells at current density of 0.2 C to 2 C. Notably, the cells with BC/ZIF-67 separator showed preferable invertibility than other separators when the discharge current density recovered from 2 to 0.2 C. At the same time, the cell with BC/ZIF-67 separator also had excellent discharge capacity at the same current density. The outstanding rate performance was related to higher ion conductivity of BC/ZIF-67 separator and lower interfacial resistance. The 10th, 20th, 30th, 40th, and 50th charge/discharge behaviors of the cells with BC/ZIF-67 separators are shown in Fig. 7c. The curves exhibited stable charging and discharging platform and less capacity loss. This was ascribed to the excellent liquid electrolyte retention capability of the BC/ZIF-67 separator. The obtained discharge profiles of cells are illustrated in Fig. 7d–f. Obviously, the discharge capacities of cells decreased as the current density increases. This was mainly due to the increased degree of ohmic polarization and serious overpotential at high discharge current density (Jeong et al. 2010a).

The EIS plots of the cells are shown in Fig. 7g, h. The semicircle in the Nyquist plots were associated with the overall resistance. The Nyquist plots also exhibited linearity at low frequency, which was mainly due to the transfer of lithium-ions (Reizabal

et al. 2020). After 100 cycles, the diameter of the semicircle increased, which also represented the increase of the overall resistance. It was worth noting that the overall resistance of the cell with the PP separator was the largest. This was due to the formation of solid electrolyte interface (SEI) layer with low ionic conductivity and the consumption of liquid electrolyte. On the contrary, the good interfacial compatibility between BC/ZIF-67 separator and electrode ensured a stable SEI layer and improved lithium deposition, thus ensuring the stable cycle performance of LIB (Xu et al. 2018). It can be seen from Fig. S4 that the lithium sheet that has not undergone the cycle test shows a flat surface. After the cycle test of the battery with PP separator, an uneven SEI layer was observed on the lithium anode. In contrast, batteries with BC/ZIF-67 separators formed a uniform SEI layer on the lithium anode after the cycle test.

Conclusions

In brief, BC/ZIF-67 separator was produced successfully by decorating ZIF-67 on bacterial cellulose nanofiber. After introducing ZIF-67 on BC membrane, the pore size and pore distribution of separator were improved. The obtained BC/ZIF-67 separator showed outstanding electrolyte retention capability and excellent wettability, thereby exhibiting high ionic conductivity (0.837 mS cm^{-1}). In addition to the advantages of environmental friendliness, BC/ZIF-67 separator also showed heat resistance than PP separator. LIB fabricated with BC/ZIF-67 separator showed excellent discharge capacity retention (91.41%) and better rate capability than other separators. Accordingly, BC/ZIF-67 separator is of great significance for the research of high-performance LIB.

Acknowledgments This research was supported by the Shandong Science and Technology Program Project (2015GGX102029).

Author contributions All authors participated in the determination of the experimental protocol and the correction of the manuscript.

Compliance with ethical standards

Conflict of interest The authors declare no competing financial interest.

References

Bu Y, Cao M, Jing Y et al (2018) Ultra-thin bacterial cellulose/poly(ethylenedioxythiophene) nanofibers paper electrodes for all-solid-state flexible supercapacitors. Electrochim Acta 271:624–631. https://doi.org/10.1016/j.electacta.2018.03.155

Carlmark A, Larsson E, Malmström E (2012) Grafting of cellulose by ring-opening polymerisation—a review. Eur Polym J 48:1646–1659. https://doi.org/10.1016/j.eurpolymj.2012.06.013

Chen P, Ren H, Yan L et al (2019) Metal-organic frameworks enabled high-performance separators for safety-reinforced lithium ion battery. ACS Sust Chem Eng 7:16612–16619. https://doi.org/10.1021/acssuschemeng.9b03854

Chen W, Liu Y, Ma Y et al (2015) Improved performance of lithium ion battery separator enabled by co-electrospinnig polyimide/poly(vinylidene fluoride-co-hexafluoropropylene) and the incorporation of TiO_2-(2-hydroxyethyl methacrylate). J Power Sour 273:1127–1135. https://doi.org/10.1016/j.jpowsour.2014.10.026

Chen P, Shen J, Wang T et al (2018) Zeolitic imidazolate framework-67 based separator for enhanced high thermal stability of lithium ion battery. J Power Sour 400:325–332. https://doi.org/10.1016/j.jpowsour.2018.08.005

Chen Y, Qiu L, Ma X et al (2020) Electrospun PMIA and PVDF-HFP composite nanofibrous membranes with two different structures for improved lithium-ion battery separators. Solid State Ion. https://doi.org/10.1016/j.ssi.2020.115253

Costa C, Lee Y, Kim J et al (2019) Recent advances on separator membranes for lithium-ion battery applications: From porous membranes to solid electrolytes. Energy Stor Mater 22:346–375. https://doi.org/10.1016/j.ensm.2019.07.024

Esho I, Shah K, Jain A (2018) Measurements and modeling to determine the critical temperature for preventing thermal runaway in Li-ion cells. Appl Therm Eng 145:287–329. https://doi.org/10.1016/j.applthermaleng.2018.09.016

Fang J, Kelarakis A, Lin Y et al (2011) Nanoparticle-coated separators for lithium-ion batteries with advanced electrochemical performance. Phys Chem Chem Phys 13:14457–14461. https://doi.org/10.1039/c1cp22017a

French A (2014) Idealized powder diffraction patterns for cellulose polymorphs. Cellulose 21:885–896. https://doi.org/10.1007/s10570-013-0030-4

Guo S, Zhang P, Feng Y et al (2020) Rational design of interlaced Co_9S_8/carbon composites from ZIF-67/cellulose nanofibers for enhanced lithium storage. J Alloys Compd. https://doi.org/10.1016/j.jallcom.2019.152911

He T, Zeng G, Feng C et al (2020) A solid-electrolyte-reinforced separator through single-step electrophoretic assembly for safe high-capacity lithium ion batteries. J Power Sour. https://doi.org/10.1016/j.jpowsour.2019.227469

Hishikawa Y, Togawa E, Kondo T (2017) Characterization of individual hydrogen bonds in crystalline regenerated cellulose using resolved polarized FTIR spectra. ACS Omega 2:1469–1476. https://doi.org/10.1021/acsomega.6b00364

Hu Y, Kazemian H, Rohani S et al (2011) In situ high pressure study of ZIF-8 by FTIR spectroscopy. Chem Commun 47:12694–12696. https://doi.org/10.1039/c1cc15525c

Huang F, Xu Y, Peng B et al (2015) Coaxial Electrospun cellulose-core fluoropolymer-shell fibrous membrane from recycled cigarette filter as separator for high performance lithium-ion battery. ACS Sustain Chem Eng 3:932–940. https://doi.org/10.1021/acssuschemeng.5b00032

Huang C, Ji H, Yang Y et al (2020) TEMPO-oxidized bacterial cellulose nanofiber membranes as high-performance separators for lithium-ion batteries. Carbohydr Polym. https://doi.org/10.1016/j.carbpol.2019.115570

Jeong H, Hong S, Lee S (2010a) Effect of microporous structure on thermal shrinkage and electrochemical performance of Al_2O_3/poly(vinylidene fluoride-hexafluoropropylene) composite separators for lithium-ion batteries. J Membr Sci 364:177–182. https://doi.org/10.1016/j.memsci.2010.08.012

Jeong H, Kim D, Jeong Y et al (2010b) Effect of phase inversion on microporous structure development of Al_2O_3/poly(vinylidene fluoride-hexafluoropropylene)-based ceramic composite separators for lithium-ion batteries. J Power Sour 195:6116–6121. https://doi.org/10.1016/j.jpowsour.2009.10.085

Jia S, Yang S, Zhang M et al (2020) Eco-friendly xonotlite nanowires/wood pulp fibers ceramic hybrid separators through a simple papermaking process for lithium ion battery. J Membr Sci. https://doi.org/10.1016/j.memsci.2019.117725

Jiang F, Yin L, Yu Q et al (2015) Bacterial cellulose nanofibrous membrane as thermal stable separator for lithium-ion batteries. J Power Sour 279:21–27. https://doi.org/10.1016/j.jpowsour.2014.12.090

Li H, Lin C, Shi J et al (2014) Preparation and characterization of safety PVDF/P(MMA-co-PEGMA) active separators by studying the liquid electrolyte distribution in this kind of membrane. Electrochim Acta 115:317–325. https://doi.org/10.1016/j.electacta.2013.10.183

Lin R, Liu S, Ye J et al (2016) Photoluminescent metal-organic frameworks for gas sensing. Adv Sci. https://doi.org/10.1002/advs.201500434

Moon J, Jeong J, Kim J et al (2019) An ultrathin inorganic-organic hybrid layer on commercial polymer separators for advanced lithium-ion batteries. J Power Sour 416:89–94. https://doi.org/10.1016/j.jpowsour.2019.01.075

Qin J, Wang S, Wang X (2017) Visible-light reduction CO_2 with dodecahedral zeolitic imidazolate framework ZIF-67 as an efficient co-catalyst. Appl Catal B 209:476–482. https://doi.org/10.1016/j.apcatb.2017.03.018

Reizabal A, Gonçalves R, Fidalgo-Marijuan A et al (2020) Tailoring silk fibroin separator membranes pore size for improving performance of lithium ion batteries. J Membr Sci. https://doi.org/10.1016/j.memsci.2019.117678

Schejn A, Balan L, Falk V et al (2014) Controlling ZIF-8 nano- and microcrystal formation and reactivity through zinc salt variations. CrystEngComm 16:4493–4500. https://doi.org/10.1039/c3ce42485e

Sheng J, Chen T, Wang R et al (2020) Ultra-light cellulose nanofibril membrane for lithium-ion batteries. J Membr Sci. https://doi.org/10.1016/j.memsci.2019.117550

Shi X, Sun Q, Boateng B et al (2019) A quasi-solid composite separator with high ductility for safe and high-performance lithium-ion batteries. J Power Sour 414:225–232. https://doi.org/10.1016/j.jpowsour.2019.01.005

Sun G, Liu B, Niu H et al (2020a) In situ welding: Superb strength, good wettability and fire resistance tri-layer separator with shutdown function for high-safety lithium ion battery. J Membr Sci. https://doi.org/10.1016/j.memsci.2019.117509

Sun X, Li M, Ren S et al (2020b) Zeolitic imidazolate framework-cellulose nanofiber hybrid membrane as Li-Ion battery separator: basic membrane property and battery performance. J Power Sour. https://doi.org/10.1016/j.jpowsour.2020.227878

Sun X, Xu W, Zhang X et al (2021) ZIF-67@Cellulose nanofiber hybrid membrane with controlled porosity for use as Li-ion battery separator. J Energy Chem 52:170–180. https://doi.org/10.1016/j.jechem.2020.04.057

Tian F, Cerro A, Mosier A et al (2014) Surface and stability characterization of a nanoporous ZIF-8 thin film. J Phys Chem C 118:14449–14456. https://doi.org/10.1021/jp5041053

Tran UPN, Le KKA, Phan NTS (2011) Expanding applications of metal-organic frameworks: zeolite imidazolate framework ZIF-8 as an efficient heterogeneous catalyst for the knoevenagel reaction. ACS Catal 1:120–127. https://doi.org/10.1021/cs1000625

Wang J, Hu Z, Yin X et al (2015) Alumina/phenolphthalein polyetherketone ceramic composite polypropylene separator film for lithium ion power batteries. Electrochim Acta 159:61–65. https://doi.org/10.1016/j.electacta.2015.01.208

Wang Z, Xiang H, Wang L et al (2018) A paper-supported inorganic composite separator for high-safety lithium-ion batteries. J Membr Sci 553:10–16. https://doi.org/10.1016/j.memsci.2018.02.040

Wang W, Yang S, Lin C et al (2020) Investigation of mechanical property of cylindrical lithium-ion batteries under dynamic loadings. J Power Sour. https://doi.org/10.1016/j.jpowsour.2020.227749

Weng B, Xu F, Alcoutlabi M et al (2015) Fibrous cellulose membrane mass produced via forcespinning® for lithium-ion battery separators. Cellulose 22:1311–1320. https://doi.org/10.1007/s10570-015-0564-8

Xu Q, Wei C, Fan L et al (2017) A bacterial cellulose/Al_2O_3 nanofibrous composite membrane for a lithium-ion battery separator. Cellulose 24:1889–1899. https://doi.org/10.1007/s10570-017-1225-x

Xu D, Wang B, Wang Q et al (2018) High-strength internal cross-linking bacterial cellulose-network-based gel polymer electrolyte for dendrite-suppressing and high-rate lithium batteries. ACS Appl Mater Interfaces 10:17809–17819. https://doi.org/10.1021/acsami.8b00034

Xue C, Jin D, Nan H et al (2020) A novel polymer-modified separator for high-performance lithium-ion batteries. J Power Sour. https://doi.org/10.1016/j.jpowsour.2019.227548

Zhan X, Zhang J, Liu M et al (2019) Advanced polymer electrolyte with enhanced electrochemical performance for lithium-ion batteries: effect of nitrile-functionalized ionic liquid. ACS Appl Energy Mater 2:1685–1694. https://doi.org/10.1021/acsaem.8b01733

Zhang T, Tian T, Shen B et al (2019a) Recent advances on biopolymer fiber based membranes for lithium-ion battery

separators. Compos Commun 14:7–14. https://doi.org/10.1016/j.coco.2019.05.003

Zhang X, Li N, Hu Z et al (2019b) Poly(p-phenylene terephthalamide) modified PE separators for lithium ion batteries. J Membr Sci 581:355–361. https://doi.org/10.1016/j.memsci.2019.03.071

Zhao J, Chen D, Boateng B et al (2020) Atomic interlamellar ion path in polymeric separator enables long-life and dendrite-free anode in lithium ion batteries. J Power Sour. https://doi.org/10.1016/j.jpowsour.2020.227773

Zhou Y, Fuentes-Hernandez C, Khan T et al (2013) Recyclable organic solar cells on cellulose nanocrystal substrates. Sci Rep. https://doi.org/10.1038/srep01536

Zhu L, Zong L, Wu X et al (2018) Shapeable fibrous aerogels of metal-organic-frameworks templated with nanocellulose for rapid and large-capacity adsorption. ACS Nano 12:4462–4468. https://doi.org/10.1021/acsnano.8b00566

Zhu G, Jing X, Chen D et al (2020) Novel composite separator for high power density lithium-ion battery. Int J Hydrogen Energy 45:2917–2924. https://doi.org/10.1016/j.ijhydene.2019.11.125